Copyright © 2005 by ABCM

AERODYNAMIC HEATING ON VSB-30 SOUNDING ROCKET

Jose Augusto Mazzoni
Instituto Tecnológico da Aeronáutica – ITA
Centro Técnico Aeroespacial – CTA
Pr. Mal. Eduardo Gomes, 50, Vila das Acácias
12228-901
jamazzoni@yahoo.com.br

José Bezerra Pessoa Filho
Instituto de Aeronáutica e Espaço – IAE
Centro Técnico Aeroespacial - CTA
Pr. Mal. Eduardo Gomes, 50, Vila das Acácias
12228-904
São José dos Campos, SP
bezerra@iae.cta.br

Humberto Araujo Machado
Instituto de Aeronáutica e Espaço – IAE
Centro Técnico Aeroespacial - CTA
Pr. Mal. Eduardo Gomes, 50, Vila das Acácias
12228-904
São José dos Campos, SP
humbertoam@iae.cta.br

Faculdade de Tecnologia - FAT
Universidade do Estado do Rio de Janeiro – UERJ
Estrada Resende-Riachuelo s/n, Morada da Colina
27523-000
Resende, RJ
machado@fat.uerj.br

Abstract. *Aerodynamic heating on the fin leading edges of a sounding rocket flying at hypersonic speed is evaluated. The fluid flow properties are obtained in an approximate fashion, whereas the convective heat flux is calculated from classical relationships provided in the literature to this type of problem. Since an ablative type of material is applied externally to the fins, a transient one-dimensional coupled conductive-change phase material problem results. The finite volume method is then used to solve the resulting equations and temperature distributions at the fin are obtained. For one of the simulations, it was possible to compare against experimental measurements, taken during the flight of VSB-30 sounding rocket. Considering the approximations used in the development of this work, as well as the uncertainties involved on the flight measurements, there was a fair agreement between the estimated values and the ones measured.*

Keywords*: aerodynamic heating, sounding rocket, heat transfer, phase change material*

1. Introduction

Sounding rockets are extensively used to study the upper layers of the earth´s atmosphere and to provide microgravity environments. The Institute of Aeronautics and Space (IAE) has designed, built and launched hundreds of sounding rockets along the past 40 years. Some of them are developed upon request of other countries´s space agencies. This is the case, for example, of VSB-30, a two-stage sounding rocket developed to be used by DLR (German Space Agency). Figure 1 shows a schematic representation of VSB-30. It has a total length of *13 m* and a diameter of *0,6 m*. It is equipped with two solid propellant motors, namely S-31 and S-30. S-31 acts like a booster during its *15 s* burning time, whereas S-30 burns for about *30 s*, reaching a maximum altitude of *300 km* approximately. During its flight VSB-30 provides *6 minutes* of microgravity environment.

Figure 2.a shows the altitude-velocity map of VSB-30 (Garcia, 2003). According to Fig. 2.a, VSB-30 reaches the speed of *6.500 km/h* while still flying within the earth´s atmosphere. Figure 2.b shows the Mach number distribution during the first *60 s* flight of VSB-30. It is worth mentioning that for practical purposes continuous flow regime is assumed to be *90 km* thick. Beyond *90 km*, it is assumed free molecular flow.

As a result of its very high speeds, aerodynamic heating arises as a major problem to be considered in the VSB-30 design. Due to the friction between VSB-30 and the atmosphere, a boundary layer results and heat is transferred from the flow to the VSB-30 external surface. This problem is larger near the stagnation regions, such as those existing at the nose cone and the fins leading edges. Figure 2.b shows the recovery temperature during the *60 s* ascend atmospheric

flight of VSB-30. Due to the air compression, caused by strong normal shocks near these regions, the air temperature surpasses *1400 °C*. As a consequence, heat is transferred to VSB-30 surface. Since such surfaces are mostly made of metals, it is mandatory to evaluate the temperature levels on these regions specifying, if necessary, an adequate thermal protection system to them.

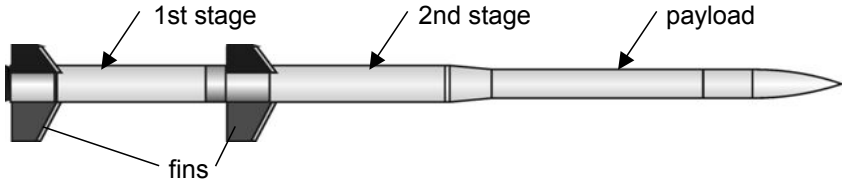

Figure 1. VSB-30 sounding rocket.

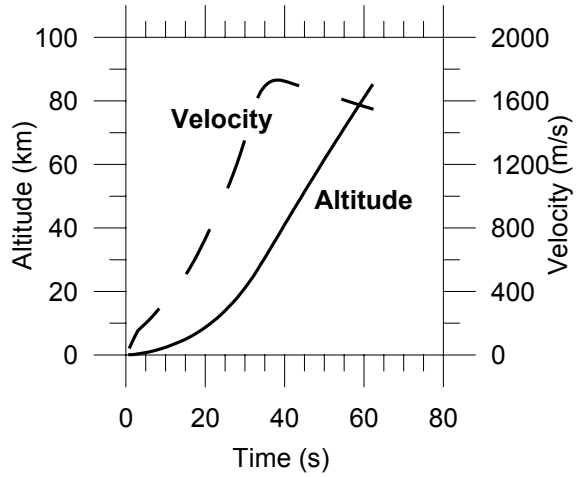

Figure 2.a. Altitude-Velocity map.

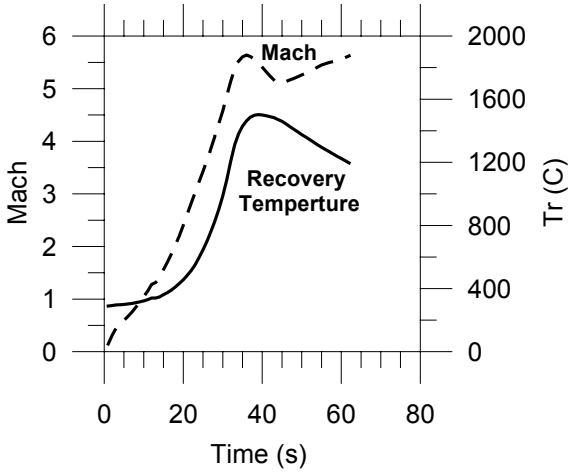

Figure 2.b. Mach number and recovery temperature.

Considering that VSB-30 is fin stabilized, i.e., the fins induces rotation around its longitudinal axis, and considering that the fins leading edge are made of *1 mm* stainless steel, this work will concentrate its effort on the estimation of the temperature levels on the 2nd stage leading edge fins. The estimated temperatures are then compared against those measured during VSB-30 flight in October 2004.

2. Formulation

2.1 Inviscid flow conditions

To predict the heat transfer on VSB-30 2nd stage leading edge fins, it is necessary to know the pressure, temperature and velocity fields around them. That can be accomplished by numerically solving the boundary layer equations. However, such a procedure is expensive and time consuming. In the present work a simpler, but reliable, engineering approach is used. The following simplifying assumptions are made:

- VSB-30 rotation around its longitudinal axis is neglected
- Physical properties are considered constant with temperature
- Atmospheric air is considered to behave as a calorically and thermally perfect gas (no chemical reactions)
- Wall heating is only by convection
- Zero angle of attack

Two different regions of the fins leading edge are considered. They are represented in Fig. 3 as point 1 and point 2 located, respectively, at the stagnation line and at *1 cm* after the intersection between the cylindrical and flat parts o the the leading edge fin.

It is assumed that the free stream conditions ahead of the fins are those given by v_∞, T_∞, p_∞, corresponding, respectively, to velocity, temperature and pressure. Thus, by knowing v_∞ and altitude, as function of time, together with an atmospheric model provided by the US Standard Atmosphere (1976), it is possible to evaluate the free stream properties, such as p_∞, T_∞, and c_∞, which represent local pressure, temperature and speed of sound, respectively.

For supersonic flow ($M_\infty > 1$), which begins at *8 s* (altitude of *2 km*), a detached shock wave appears ahead of the fin. By using the normal shock relationships available in the literature (Anderson Jr., 1982), it is possible to calculate v_1, T_1 and p_1 after the shock, point 1. To evaluate v_2, T_2 and p_2, oblique shock equations are used (Anderson Jr., 1982).

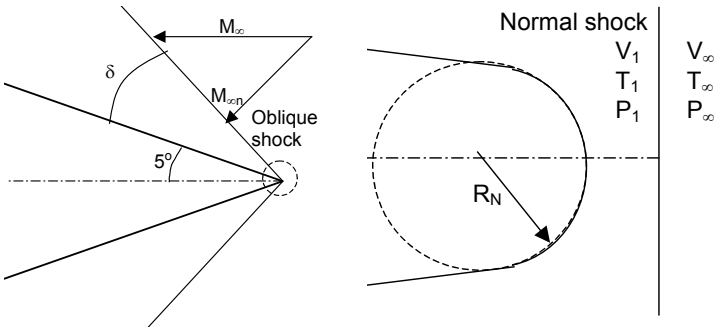

Figure 3. Schematic representation of the leading edge cross section.

2.2 Convective heat transfer to the fins

Due to the strong shock near the leading edge of the fin, the temperature behind the shock gets high. Figure 2.b shows the recovery temperature at the stagnation line, corresponding to point 1 of Fig. 3. The recovery temperature is given by

$$T_r = T_1\left[1 + r\frac{(\gamma-1)}{2}M_1^2\right] \tag{1}$$

where T_1 and M_1 are the static temperature and Mach number behind the shock, r is the recovery factor given by $r = \sqrt{\Pr}$ and $r = \sqrt[3]{\Pr}$, for laminar (point 1 of Fig. 3) and turbulent flow (point 2 of Fig. 3), respectively. As a consequence of the high temperature behind the shock, heat will be transferred from the fluid flow to the fin. According to van Driest, the convective heat transfer at the stagnation line is given by (Anderson Jr., 1989)

$$q_1 = 0.570\ \Pr^{-0.6}(\rho_1\mu_1)^{1/2}\sqrt{\frac{du_1}{dx}}Cp\,(T_r - T_w) \tag{2}$$

where

$$\frac{du_1}{dx} = \frac{1}{R_N}\sqrt{\frac{2(p_1 - p_\infty)}{\rho_\infty}} \tag{3}$$

The use of Eq. (2) corresponds to the assumption of a supersonic flow against a unswept circular cylinder of radius R_N, (R_N= *3 mm*). T_w refers to the wall temperature.

At point 2 of Fig. 3, flow over a flat plate is assumed together with the Reynolds analogy. Thus, at point 2 the convective heat transfer is obtained from (Anderson Jr., 1989):

$$q_2 = \rho_2\, V_2\, Cp\,(T_r - T_w)\, C_h \tag{4}$$

where

$$C_h = 0.0296\left(\mathrm{Re}_x^*\right)^{-0.2} \qquad \text{and} \qquad \mathrm{Re}_y^* = \frac{\rho^*\, v_2\, y}{\mu^*} \tag{5.a, b}$$

In evaluating the Reynolds number, Re^*, ρ and μ are calculated at Eckert's reference temperature, given by (Anderson Jr., 1989):

$$T^* = T_2\left[1 + 0.032M_2^2 + 0.58\left(\frac{T_W}{T_2} - 1\right)\right] \tag{6}$$

It is worth mentioning that ρ_2, v_2 , M_2 and T_2 are obtained from the oblique shock relationships. The viscosity, μ, is evaluated according to Sutherland´s law (Anderson Jr., 1989). In Eq. (5.b), y is measured from the intersection between the cylindrical and the flat plate ($\varphi_o = 36{,}6^o$), as shown in Fig. 4.

2.3. Fins Temperature

Having determined the flow properties and the heat flux at the wall, Eqs. (2) and (4), it is possible to calculate the temperature of the fin. Considering the small radius of curvature of the fin leading edge, R_N= *3mm*, its small thickness, *1 mm*, and the fact that they are made of stainless steel, Tab. 1, an ablative type of material, FIREX RX-2376, is applied externally to the surface of the fin. The physical configuration is schematically shown in Fig. 4.

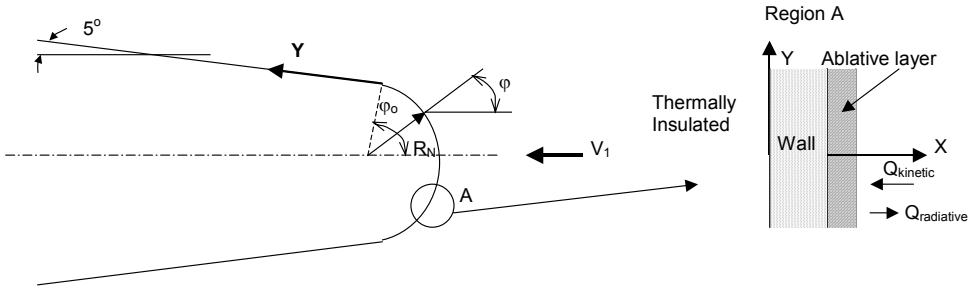

Figure 4. Coordinate system near the fin´s leading edge.

To evaluate the temperature of the fin, a one-dimensional slab is considered to represent the fin, Figs. 5. The backside of the fin is assumed to be insulated, whereas a time-dependent convective heat flux, $q(t)$, is applied externally to the fin. The external surface is also allowed to radiate heat. Due to the application of an ablative type of thermal protection to the fin, three different situations may occur, namely: Pre-ablative period, Ablative period and Pos-ablative period, Figs. 5.

Table 1. Properties of stainless steel (Peterson, 1994).

Emissivity	*0.11*
Specific heat	*500 J/kg K*
Thermal conductivity	*16.2 W/m K*
Density	*8000 kg/m^3*

Table 2. Properties of FIREX RX-2376 (Pyrogenics Group, 2003).

Heat of ablation	*4.2 MJ/kg*
Ablative temperature	*138^o C*
Specific heat	*1,674.6 J/kg K*
Thermal conductivity	*0.24 W/m K*
Density	*1,170.2 kg/m^3*

During the pre-ablative period, heat is transferred to the fin, but its external surface temperature is lower than the FIREX ablative temperature (*138 ^{o}C*, Tab. 2). This situation is schematically represented in Fig. 5.a and the physical domain can be divided into two parts. For the stainless steel wall the overall energy conservation equation yields

$$\frac{\partial T_{ss}}{\partial t} = \alpha_{ss} \frac{\partial^2 T_{ss}}{\partial x_{ss}^2} \tag{7}$$

$$\left.\frac{\partial T_{ss}}{\partial x_{ss}}\right|_{x_{SS}=0} = 0 \; ; \qquad T_{SS}(t,x_w) = T_F(t,0) \tag{8.a,b}$$

where T_{ss} and α_{ss} are the stainless steel temperature and thermal diffusivity, x_{ss} is the x-coordinate along the stainless steel thickness, x_w is the coordinate of the stainless steel-FIREX interface, and $T_F(t,0)$ is the FIREX temperature, at the interface. For the FIREX layer, the conservation of energy provides

$$\frac{\partial T_F}{\partial t} = \alpha_F \frac{\partial^2 T_F}{\partial x_F^2} \tag{9}$$

Here x_F is the x-coordinate along the FIREX layer, Fig. 5.b, and x_{i0} is the initial FIREX thickness, Fig. 5.a. The boundary conditions for the FIREX layer are given by:

$$-k_F \left.\frac{\partial T_F}{\partial x_F}\right|_{X_F = X_i(t)} = h(t,y)\left[T_F(t,x_i) - T_R\right] + \varepsilon\,\sigma\left[T_F^4(t,x_i) - T_\infty^4\right] \; ; \qquad T_{SS}(t,x_w) = T_F(t,0) \tag{10.a,b}$$

where k_F represents the thermal conductivity of FIREX, and h is the convection heat transfer coefficient obtained from Eqs. (2) and (4). T_∞ is the atmospheric temperature. It is worth mentioning that the coupling between the two sets of equations, is given by Eq. (8.b) and Eq. (10.b).

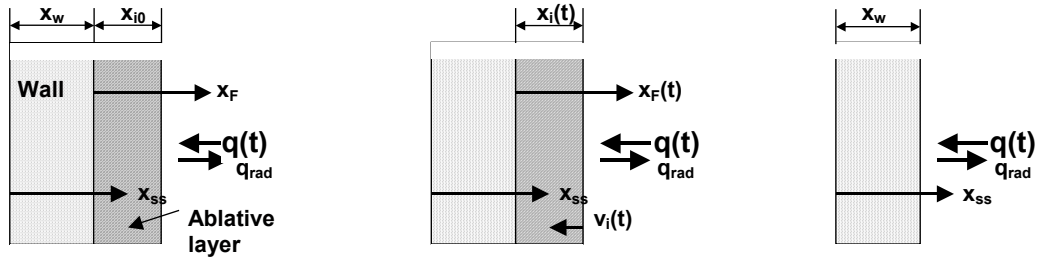

(a) Pre-ablative period (b) Ablative period (c) Pos-ablative period

Figure 5. Coordinate system for the conductive and ablative processes.

Once FIREX external surface reaches *138 °C*, Tab. 2, it becomes liquid and it is assumed to be instantaneously removed out of the surface by the high speed flow. In other words, when $T_{FF}(t,x_{i0}) = 138\ ^oC$ the ablative process begins and the application of the energy conservation principle yields (Arpaci, 1991)

$$\frac{\partial T_F}{\partial t} = \eta^2 \alpha_F \frac{\partial^2 T_F}{\partial x_F^2} \tag{11}$$

where $\eta = x_i(t)/x_{i0}$ is the time-dependent correction factor for the x-coordinate, applied to the ablative layer. The use of such a correction factor is a way for keeping the same number of volume elements within the FIREX domain during the ablative period. During this period, the boundary condition at the stainless steel-FIREX interface is the same as Eq. (10.b). At $x_F = x_i(t)$, Fig. 5.b the boundary condition is given by

$$T_F(t,x_i) = T_a \tag{12}$$

where T_a is the FIREX ablative temperature.

By applying an energy balance at the FIREX external moving surface, it is possible to obtain the regression velocity of its surface, Fig. 5.c, namely

$$v_i(t) = \frac{h(t,y)\left[T_F(t,x_i) - T_R\right] + \varepsilon\sigma\left[T_F^4(t,x_i) - T_\infty^4\right] + k_F \left.\dfrac{\partial T_F}{\partial x_F}\right|_{X_F = X_i}}{\rho_F L} \tag{13}$$

where ρ_F is the FIREX density and L is its heat of ablation, Tab. 2. Once the ablation velocity is known, the position of the surface, at any time, $x_i(t)$, can be obtained as

$$\frac{dx_i}{dt} = v_i \tag{14}$$

If the ablative material is not totally removed out of the surface, the fin temperature is given by solving Eqs. (7)-(14). On the other hand, if the total heat applied to the surface is enough to remove all the FIREX, a transient, one-dimensional conduction problem results, as represented by Eqs. (7) and (8.a). In this case, however, Eq. (8.b) is substituted by the following boundary condition

$$-k_{ss} \left.\frac{\partial T_{ss}}{\partial x_{ss}}\right|_{X_{ss} = X_w} = h(t,y)\left[T_{ss}(t,x_w) - T_R\right] + \varepsilon\sigma\left[T_{ss}^4(t,x_w) - T_\infty^4\right] \tag{15}$$

At time equal to zero:

$$T(x,0) = T_\infty \tag{16}$$

Equations (7-16) are resolved through Finite Volume Method and an explicit FTCS scheme is used (Maliska, 1995).

3. Flight measurements

During VSB-30 flight, four temperature measurements were taken at different locations of the fin leading edge, Fig. 6. The locations of the sensors correspond to point 2 of Fig. 3. PT 100 thermo sensors were used (Fraden, 1996). Figure 7 shows the measured temperatures. It is worth mentioning that a layer of ablative material was applied to the fins. Due to limitations of the application procedure, the thickness of the ablative material applied on the fins may vary between *0.40 mm* and *0.85 mm*.

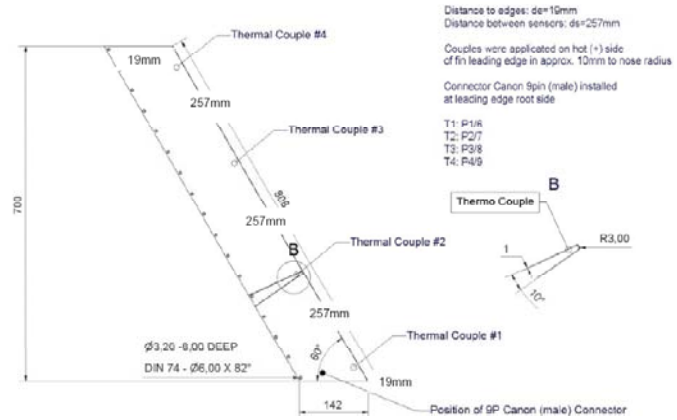

Figure 6. Location of the temperature sensors along VSB-30 2nd stage fin leading edge.

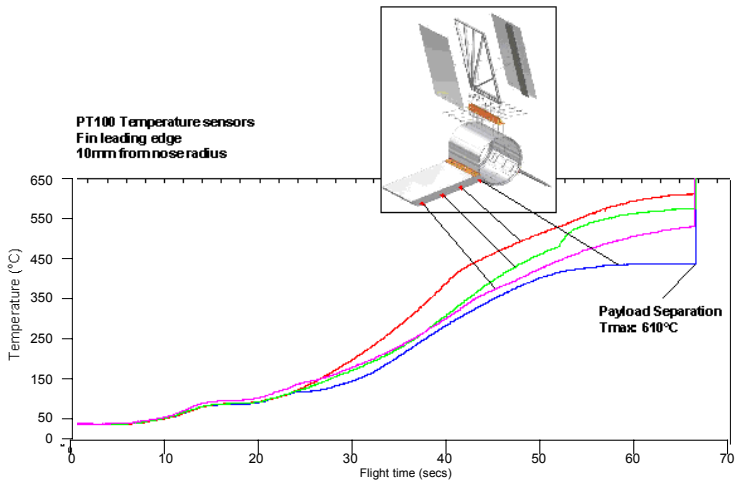

Figure 7. Temperature distributions with time at the four locations considered.

4. Results

4.1 Stagnation line

By using the trajectory presented in Fig. 1 and the approximated theoretical procedure outlined in section 2, the transient temperature at the external surface of the fin was obtained, Fig. 8.a. Three different cases were considered, namely: ***Case 1:*** fin without ablative material; ***Case 2:*** fin covered with *0.40 mm* of FIREX; and ***Case 3:*** fin covered with *0.85 mm* of FIREX. Due to the high thermal diffusivity of the stainless steel, the temperature difference across its *1 mm* thickness is lower than *0.5 °C*. As it is shown in Fig. 8.a, the use of FIREX did not have a significant effect on decreasing the maximum temperature of the fin, which occurred around *45 s* of the flight. Such a behavior can be explained by the high heat flux occurring at the stagnation line, Fig. 8.b, which causes the ablative material to be totally removed out of the surface. Indeed, for ***Case 2*** the FIREX is totally consumed between *19 s* and *26 s*. For ***Case 3***, it takes *10 s* (between *19s* and *29 s*) for the FIREX to be ablated. At these times, Fig. 8.b, the convective heat flux at the stagnation line is still very high. This high heat flux is a result of the high speed flow around the fin, combined with the small radius of curvature of the fin leading edge, R_N=*3mm*. From Eqs. (2) and (3), it is observed that $q_o \propto 1/\sqrt{R_N}$. Such a high heat flux, applied to a thin wall (*1 mm*) causes a maximum temperature to reach *1300 °C* at the surface of the fin, ***Case 1***. The use of a *0.40 mm* thickness FIREX on the surface of the fin delayed the beginning of the increase on temperature of the fin to *26 s*, Fig. 8.a, but it did not have a significant effect on decreasing the fin maximum temperature, ***Case 2***. Such a behavior is explained by the amount of FIREX used, as well as by its low ablative temperature, *138 °C*. When a *0.85 mm* thick FIREX layer is applied to the fin, the maximum temperature is decreased by *100 °C* and the beginning of the temperature increase on the fin is delayed to *29 s*, ***Case 3***. The reasons for such a

behavior are the same as those for ***Case 2***. The measurement of these temperatures was not taken during the VSB-30 flight because of the difficulties associated with the fixation of the sensors at this location.

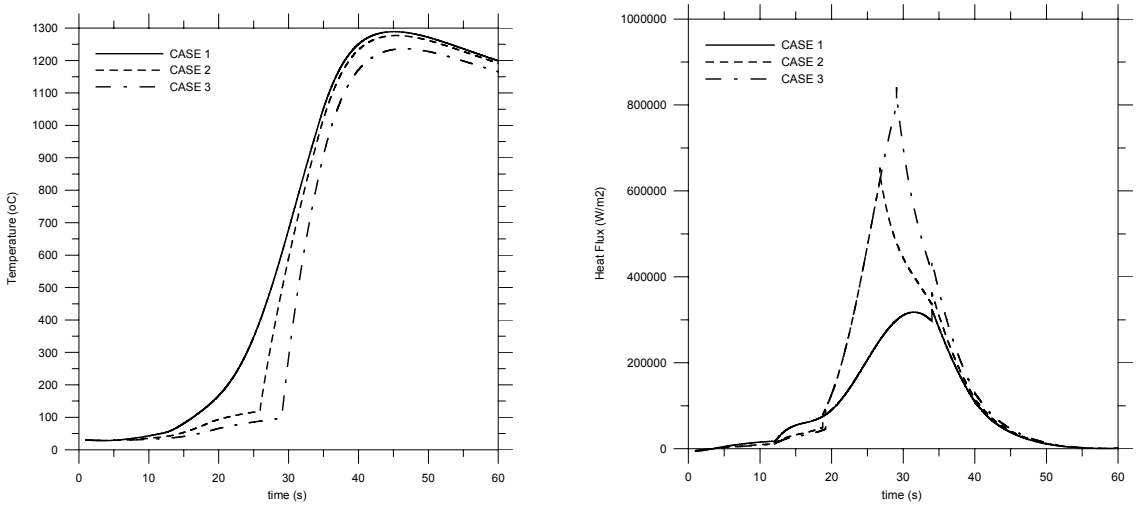

(a) Temperature (b) Heat Flux

Figure 8. Temperature and heat flux at the stagnation line, point 1.

4.2 Leading edge

Temperature distributions were obtained at the leading edge of the fin, corresponding to point 2 in Fig. 3, which is located at *1cm* from the stagnation line. Once again, three different cases were considered. The results are presented in Fig. 9.a, together with the convective heat flux, Fig. 9.b. ***Case 1*** is represented by a continuous line in Fig. 9.a. It corresponds to the situation in which no FIREX is applied to the fin. The maximum estimated temperature for this case is about *750 ^oC*, occurring at *40 s*, approximately. After this time, the convective heat transfer becomes lower, Fig. 9.b, and radiative emission causes a little decrease on the temperature of the fin. The application of a *0.40 mm* thick FIREX layer on the fin leading edge, corresponding to ***Case 2***, decreases the maximum temperature by nearly *200 ^oC*. In this case, the ablative material is totally consumed between *20 s* and *30 s*. Fig. 9.b shows that this is exactly the time period in which the convective heat flux reaches its peak. Therefore, the application of FIREX in this case provides a good thermal protection to the fin. When a *0.85 mm* thick FIREX layer is used, ***Case 3***, the ablation also starts at *20 s*. However, due to the FIREX high heat of ablation, the heat load imposed to the thermal protection system is not enough to remove it out of the surface. In fact, at *60 s* of flight a *0.03mm* layer of FIREX still remains on the surface, keeping its temperature equal to *138 ^oC*.

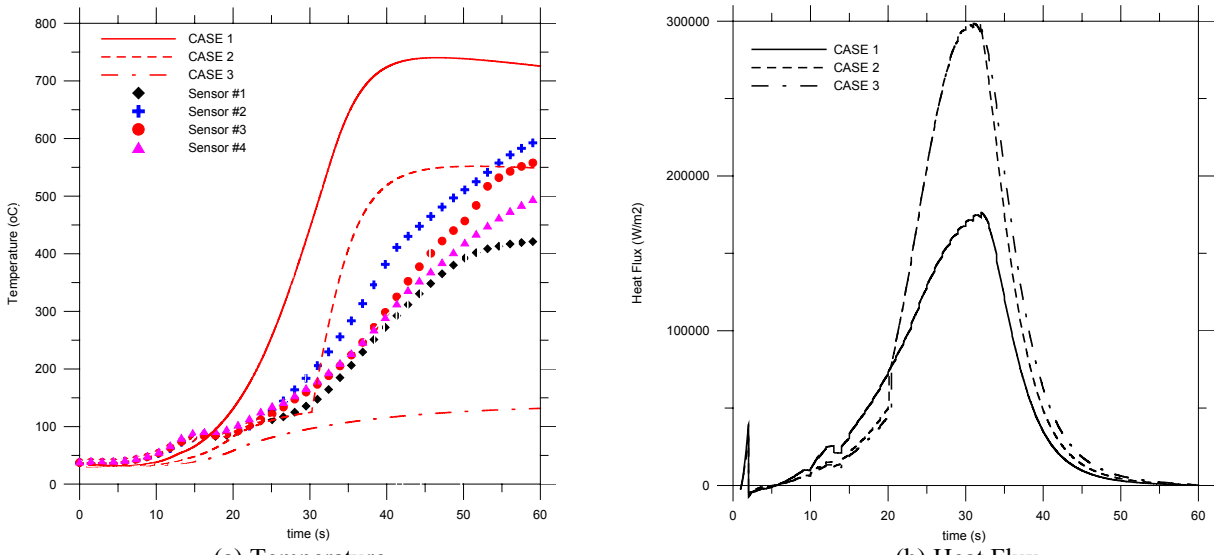

(a) Temperature (b) Heat Flux

Figure 9. Temperature and heat flux at the stagnation line, point 2.

The experimental curves show a smoother increase in temperature, as compared to the theoretical ones, Fig. 9.a. Such a behavior is believed to be related to the conduction heat transfer occurring in the y-direction, Fig. 4, and not taken into account in the present modeling. From Fig. 9.a it is observed that temperature varies significantly along the fin´s leading edge. Indeed, the measurement taken by sensor 2, Fig. 6, shows a maximum temperature about 50% higher as compared to sensor 1 (located near the fin´s base). Such a behavior is due to the three-dimensional characteristics of the fluid flow around the fin. By comparing the result shown in Fig. 8.a to the one presented in Fig. 9.a, it is noticed that predicted temperature of the fin is strongly dependent on the sensor location. At the stagnation line the maximum temperature reaches *1300 ^oC*, whereas at *1 cm* from the leading edge, it decreases to *750 ^oC*. Such a result reveals that the sensors must be precisely fixed on the fins. The numerical results presented in Fig. 9.a also shows how significant are the effects of the thickness of the ablative material applied to the fin. In fact, by changing the thickness of the ablative material from *0.40 mm* to *0.85 mm* the external temperature varies from *550 ^oC* to *138 ^oC*. It is worth mentioning, however, that the inclusion of the change phase material phenomenon into the modeling was carried out after the flight. As a consequence, in order to be able to fairly compare the theoretical predictions to the experimental measurements, an additional care must be taken in controlling the thickness of ablative material applied to the fin.

5. Conclusions

The aerodynamic heating on VSB-30 sounding rocket leading edge fin was evaluated via an approximated method. The application of an ablative type of material on the fins leading edge was considered resulting in the modeling of a transient, one-dimensional conductive-phase change material problem. One of the obtained results was compared to the experimental data obtained during a VSB-30 actual flight. If one considers the approximations involved in the modeling and the uncertanties on the ablative material thickness and location of the temperature sensors, it can be concluded that a fair agreement was obtained. The obtained results showed that the application of the thermal protection system on the leading edge of the fins did protect it against the high convective heat flux. However, at the staganation line itself, it had little effect. In a next study the modeling of two-dimensional conduction-phase change material shall be considered. The techique for fixing the temperature sensors, as well as for applying the ablative coating on the fins shall also be improved.

6. Acknowledgements

The authors would like to acknowledge the financial support provided by CNPq during the development of this work. Acknowledgments are also due to Mr. Eduardo Dore Roda, VSB-30 coordinator, for providing the experimental data presented in this work.

7. References

Anderson Jr., J. D., 1989, Hypersonic and High Temperature Gas Dynamics, McGraw-Hill.
Anderson Jr., J. D., 1982, Modern Compressible Flow, McGraw-Hill.
Arpaci, V.S., 1991, Conduction Heat Transfer, Abridge Edition.
Fraden, J., 1996, Handbook of Modern Sensors, Springer, Berlin.
Garcia, A., 2003, Cálculo da Trajetória do VSB-30, Memotec 040-ASE, IAE/CTA.
Maliska, C. R., 1995, Transferência de Calor e Mecânica dos Fluidos Computacional, LTC, Rio de Janeiro.
Pyrogenics Group, 2003, http://www.pyrographite.com.
Peterson, G. P., 1994, An Introduction to Heat Pipes, Wiley Inter-Science, NY
U.S. Standard Atmosphere, 1976.

8. Responsibility notice

The authors are the only responsible for the printed material included in this paper.